Article

Combined TPEF and SHG Imaging for the Microstructural Characterization of Different Wood Species Used in Artworks

Alice Dal Fovo [1],*, **Sara Mattana** [1], **Marco Marchetti** [2,3], **Monica Anichini** [4], **Alessio Giovannelli** [5], **Enrico Baria** [1], **Raffaella Fontana** [1] **and Riccardo Cicchi** [1,3]

1   National Research Council, National Institute of Optics (CNR-INO), Largo E. Fermi 6, 50125 Firenze, Italy; sara.mattana@ino.cnr.it (S.M.); enrico.baria@ino.cnr.it (E.B.); raffaella.fontana@ino.it (R.F.); riccardo.cicchi@ino.cnr.it (R.C.)
2   Department of Physics, University of Florence, Via G. Sansone 1, 50019 Sesto Fiorentino, Italy; m.marchetti@l4t.it
3   European Laboratory for Non-Linear Spectroscopy (LENS), Via N. Carrara 1, 50019 Sesto Fiorentino, Italy
4   National Research Council, Institute of BioEconomy (CNR-IBE), Via Madonna del Piano 10, 50019 Sesto Fiorentino, Italy; monica.anichini@ibe.cnr.it
5   National Research Council, Research Institute on Terrestrial Ecosystems (CNR-IRET), Via Madonna del Piano 10, 50019 Sesto Fiorentino, Italy; alessio.giovannelli@cnr.it
*   Correspondence: alice.dalfovo@ino.cnr.it

Abstract: The morphological and chemical conformation of wood microstructures is characteristic of individual species and strongly influences the macromechanical properties of the material, as well as its sensitivity to deterioration factors. Noninvasive techniques enabling the visualization of wood microstructures, while simultaneously providing compositional information, can significantly facilitate the analysis of wooden artworks for conservation purposes. In this paper, we present the application of combined two-photon excited fluorescence (TPEF) and second-harmonic generation (SHG) imaging as a versatile diagnostic tool for the microcharacterization of three hardwood species never analyzed by this method. Multimodal mapping of the molecular constituents based on the detected nonlinear signals provides useful information for studying the biological and biochemical deterioration of wood, opening a new field of application for a well-established and widely used imaging technology.

1. Introduction

Wood has been used extensively since ancient times with both a structural and decorative function in a variety of art objects, ranging from sculptures to paintings and musical instruments. The multiscale and anisotropic structure of wood is highly hygroscopic due to the presence of differently oriented pores, for which the peculiar size and shape are key parameters for differentiation among wood species [1,2]. Given the importance of cell walls in the growth and morphogenesis of the microstructures, it is of great interest to investigate how molecular components are organized in the three dimensions [3]. The geometry of the microstructures determines the accessibility of degradative organisms and substances and, thus, is strictly related to biological and biochemical degradation [4]. Moreover, the sensitivity of wood cells to environmental changes can be monitored based on the alterations occurring at the molecular level, which strongly influence the macromechanical properties of the timber or wood products [5].

The main chemical components of wood cells, namely cellulose, hemicellulose, and lignin, are characterized by nonlinear optical (NLO) properties, which can be exploited to obtain morphological, structural, and compositional information on the microstructures [6–8]. NLO microscopies are well-established 3D imaging techniques that have been

widely applied in the biological field for the label-free nondestructive investigation of physio-pathological processes in live samples at a subcellular spatial resolution [9]. The combined use of different NLO microscopy modalities, such as two- and three-photon excited fluorescence (TPEF [10] and 3PF [11,12]) and second- and third-harmonic generation (SHG [13] and THG [14]), provides complementary information based on the detection of fluorophores (by TPEF and 3PF), crystalline or highly organized structures without inversion symmetry (by SHG), and local differences in refractive index and dispersion, i.e., interfaces (by THG) [15]. Nonlinear processes are generated through the interaction of atoms and/or molecules with two or more photons within the same quantum event. Being second- or higher-order optical processes, their inherent low probability to occur requires a high spatial and temporal density of photons, which is typically achieved with tightly focused ultrashort-pulsed lasers. Nonlinear processes allow using near-infrared photons for exciting molecular transitions, which are typically located in the blue/UV spectral range. The major advantage, compared to linear optical techniques, is that nonlinear optical signals (SHG, THG, TPEF, and 3PF) can be generated at higher penetration depths (exceeding 500 µm in biological tissues [16]) due to the reduced light scattering and absorption of the infrared excitation wavelengths [9]. Furthermore, given the square or cubic dependence of the signal on excitation intensity, the efficient nonlinear interaction is typically confined to a femtoliter region around the focal point, as only ballistic photons contribute to the excitation process. This enables high-resolution sectioning with drastically diminished out-of-focus damages. The noninvasiveness of the technique, which is a crucial requirement in artwork diagnostics, can be ensured by simply monitoring the variation in TPEF signal intensity as a forewarning of photochemical changes inside the focal volume of the laser beam [17].

The microstructure of wood consists of cells arranged along the axis of the trunk and developed with the parenchyma rays from the core of the tree to the bark (Figure 1) [18]. Cellular arrangement and morphology determine substantial anatomical differences between softwoods—i.e., gymnosperms (conifers)—and hardwoods—i.e., angiosperms (flowering plants) (see Section 2.2. Microstructural Features) [19].

The supramolecular conformation of cellulose, which resembles that of collagen in both morphology and symmetry, may yield a strong SHG signal similar to collagen due to the hierarchical structure and the parallel orientation of the composite molecular chains. Furthermore, the strong birefringence and chirality of the polysaccharide chains of cellulose may significantly increase SHG intensity, which is another similarity with the array of polypeptides in collagen [20]. The generation of SH from cellulose is also strongly dependent on the orientation of microfibrils, which develop predominantly along the axis of longitudinal arrays of cells [20].

Another possible source of an SHG signal in wood is starch, a mixture of the two polysaccharides amylose and amylopectin. Within the stem, starch is stored in large amounts in the companion cells of the phloem (inner side of the bark) and in the parenchyma ray of the xylem. Starch represents a long-term carbon reserve in a wide variety of organisms, such as seeds and tubers, and a temporary reserve in photosynthetic tissues, specifically in chloroplasts. In particular, Amylose is often highly crystalline and, thus, is likely to generate second-harmonic signals [8]. Starch emits stronger SHG signals than cellulose due to the reverse orientation of glucose residues in the polysaccharidic chains [21,22]. Therefore, SHG imaging of cellulose requires rather high laser powers (above optimal values for live cell imaging), whereas starch can be easily imaged at laser fluencies compatible with extended cell viability.

Cell walls exhibit natural fluorescence due to the presence of lignin [23]. The emission covers a broad spectral range (blue, green, and red) depending on the excitation wavelength (with maximum absorbance by lignin at 280 nm) and on the pH of the molecular environment [24]. The fluorescence can differ significantly in hardwood and softwood species both in terms of intensity and spectral emission [25,26]. It has been observed that fluorescence from lignin can also be generated nonlinearly, namely through three- and

two-photon absorption at 840–860 nm [8,27]. While lignin is the predominant fluorophore in cell walls, the polysaccharide components, such as cellulose and starch, are considered not fluorescent [28].
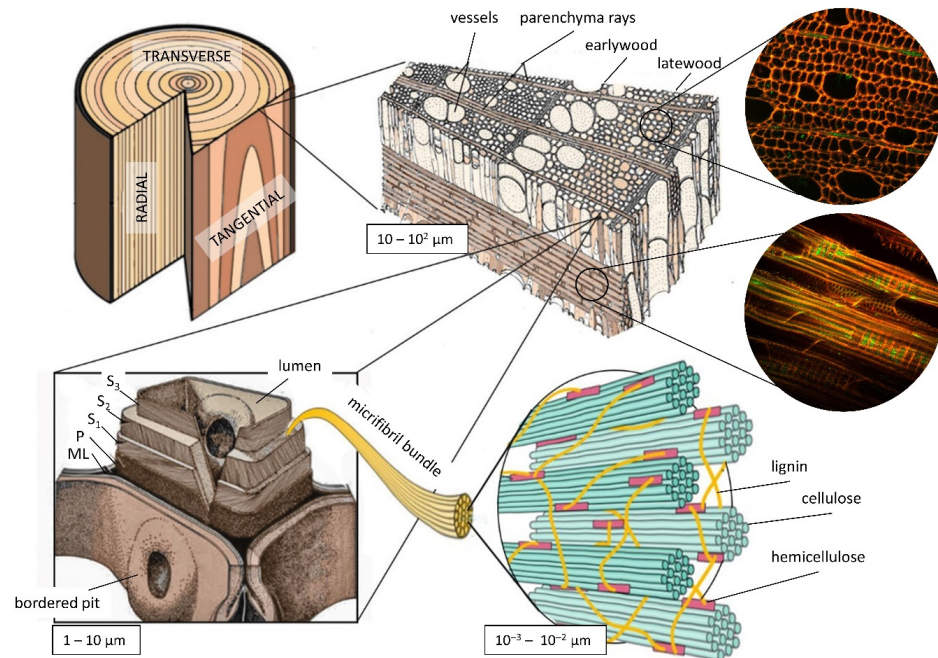
Figure 1. Wood sections at the macroscale (**top left**); schematic microstructure of hardwood species (**top middle**) with NLO images (diameter = 200 μm) of the microstructure of poplar xylem in transverse and radial sections (**top right**). Schematic representation of cell wall layers—ML, middle lamella; P, primary cell wall; S1, S2, and S3, sublayers of secondary cell wall (**bottom left**); close up of a microfibril bundle from S2 showing individual crystallites of cellulose glued together by the interfibrillar compounds of hemicellulose and lignin (**bottom right**).

To the best of our knowledge, the first 3D imaging of wood microstructures on an artistic object was performed in 2009, with a purposefully developed time-domain OCT system, based on an illumination source centered at 650 nm and reaching axial and transverse resolutions of 1.5 and 1 μm, respectively [18]. However, the visualization of wood cells provided by OCT tomograms lacked any chemical information. To overcome such a limit, some years later, the same author applied TPEF and SHG on thin shavings of acer wood and a historical violin, obtaining both the imaging and the chemical characterization of wood microstructures [27]. Although SHG emissions are generally more efficient in the forward direction due to phase-matching conditions, it was demonstrated that the SH signal can also be recorded in the backward direction when it is enhanced by specific structures or backscattered in thick scattering wood samples [29].

In this work, we extended the application of TPEF-SHG imaging to three hardwood species widely used in art production—poplar, beech, and chestnut—that have never been analyzed with these modalities. Nonlinear signals, collected in epi-detection, were combined into intensity images to differentiate and quantify chemical components. The purpose of this study is to provide a noninvasive and effective tool for the rapid recognition of wood species used in art production based on compositional and morphological information at the micrometer level that can be profitably used for conservation and restoration purposes.

2. Materials and Methods

2.1. Samples

Wood shavings were collected from mature trees of poplar (*Populus tremula* L.), beech (*Fagus sylvatica* L.), and chestnut (*Castanea sativa* M.) growing in a mixed forest in northern

Tuscany, Italy. Prismatic wood samples ($15 \times 10 \times 5$ mm^3) were obtained by notching a piece of stem with a blade in the tangential direction (Figure 1). The wood shavings were stored for a week at 4 °C before the analysis. To test the applicability of the method on CH objects without sampling while fulfilling the noninvasiveness requirements, the samples were analyzed without any pretreatment, even if the addition of a solution of glycerine and water would have eased the observation of the microstructures [30].

2.2. Microstructural Features

The major components of the physical and chemical properties of wood are the distribution and number of different cell types, namely tracheids (constituting around 90% of the volume of softwood), vessels, parenchyma, and fibers (the main components in hardwoods) [31]. The latewood, also called summerwood, can be distinguished from earlywood or springwood because of the smaller radial dimensions of the cells and the thicker walls, which also is reflected in the higher density of the bulk. A further diagnostic element for the differentiation of wood species is the presence of isolated interruptions inside the cell walls of xylem conduits (i.e., vessels and tracheids), called "pits", which connect different cells for the transfer of sap. The pit membrane has a key function in the overall hydraulic efficiency of plants, allowing water to diffuse between conduits but limiting the spread of embolism and vascular pathogens. The shape and dimension of pits significantly vary depending on the type of adjacent cells and, therefore, can be considered distinctive features of the wood species [32]. Looking more deeply into the microstructures, plant cells show a globular, elongated bag shape. The cell wall is a membrane composed of different layers, namely the primary (P) and the secondary (S) layers, which in turn is composed of three sublayers: S1, S2, and S3 (Figure 1). Adjacent cells are connected by an additional layer, called the middle lamella (ML). Inside the cell wall, laminar crystallites of cellulose are organized in microfibrils, which are embedded in a complex matrix of variously amorphous polysaccharides (hemicellulose), cross-linked with lignin, a condensed polymer of coniferyl, sinapyl, or p-coumaryl alcohol (Figure 1) [31,33]. Cellulose is a linear chain of polysaccharidic molecules linked by β-(1–4) glycosidic bonds displaying a twofold ribbon conformation. Many packing arrangements of the polysaccharidic chains are possible, and all are classifiable in cellulose I (the most abundant type, with parallel chains) and II (with antiparallel chains) [34]. Cellulose I naturally occurs in two distinct crystalline forms, Iα and Iβ, showing triclinic and monoclinic symmetry, respectively. These well-ordered molecular chains are predominantly located in the secondary cell wall in variable proportions and crystallize into the thermodynamically stable microfibrils, with a typical diameter ranging from 1.2 to 4.8 nm and lengths between 60 and 150 nm [35]. The distribution of the microfibrils differs in quantity and arrangement depending on their location in the cell wall. While the content of cellulose is about the same in both softwood and hardwood, exceeding approximately 40–45% in weight of the dry matter in most wood species, lignin is present in different quantities (usually ranging from 18% to 25% in hardwoods and from 25% to 35% in softwoods).

2.3. Nonlinear Setup

The nonlinear setup used for the analysis was developed at CNR-INO and is equipped with a dual-output Yb-based fiber fs-laser (Chameleon Discovery, Coherent Inc., Santa Clara, CA, USA). A detailed description of the system can be found elsewhere [36]. Based on previous applications of NLO on wood microstructures [27], the excitation wavelength was set at 840–850 nm (depending on the wood species), with a pulse duration of 140 fs and a repetition rate of 80 MHz, and with the power on the specimen ranging from 30 to 50 mW. Nonlinear signals coming from the sample were epi-collected using a Plan Apochromat20× objective lens (NA 0.75, WD 1 mm, Nikon, Nikon Minato, Tokyo, Japan) and detected with two photomultiplier tubes (H7422-40, Hamamatsu, Hamamatsu City, Japan) for simultaneous TPEF and SHG detection. A dichroic beam splitter filter with a 452 nm cutoff wavelength (FF452-Di01, Semrock Inc. New York, NY, USA) was used

for separating TPEF from SHG. In more detail, the TPEF signal was transmitted by the dichroic and detected without any additional emission filters, which is in agreement with previous observations on TPEF emission's spectral range of lignin [27]; the SHG signal was reflected by the dichroic and then filtered with a narrow band-pass filter centered at 420 nm (BrightLine 420/10–25 nm, Semrock Inc., New York, NY, USA). For each analyzed area, the TPEF and SHG signals were detected and displayed as intensity images, which were merged with a Java image processing software (see Figure S1 in the Supplementary Materials). Specifically, the TPEF and SHG images were assigned to the green and the red channels, respectively, thus enabling the distinction among components generating the different nonlinear signals (mainly starch, cellulose, and lignin) in a single image, as well as allowing for the visualization of micrometric features that are characteristic of each species.

3. Results

3.1. Poplar (Populus tremula L.)

The microanalysis of poplar shavings (tangential section) revealed the peculiar size and shape of the cells composing this species (Figures 2 and 3). The observed vessels, which are uniformly distributed along the ring with dimensions slightly varying between latewood and earlywood zones, were relatively small (50–100 μm), with circular or polygonal shapes. The parenchyma rays, mostly mono-seriated, showed homogenous shapes and sizes, which are typical of poplar. Bordered pits organized in lines, probably connecting fibers and vessels, were also observed. Their size, between 10 and 15 μm, is typically larger than in other wood species. The greyscale intensity images (Figure 2a,b), obtained by optically summing all excited nonlinear signals, highlight the organization of pits, demonstrating that NLO microscopy can be used to noninvasively assess wood microstructure with high resolution. A more detailed analysis can be performed by separating the two nonlinear contributions: The merged TPEF/SHG image (Figure 2c) shows similar microstructures while providing additional molecular information based on the specific nonlinear contrast mechanism. The observed fluorescence signal (green-coded in the image) is predominant and indicative of the presence of lignin. Specifically, fluorescence emission can be ascribed to syringyl p-hydroxybenzoate lignin, which in poplar is localized in the inner secondary fiber wall [25]. In the analyzed area, the SHG signal is almost absent except for some traces (red spots) inside the pits (Figure 2c) that are ascribable to starch grains, which are stored in the parenchyma rays and are visible through the pit membrane.
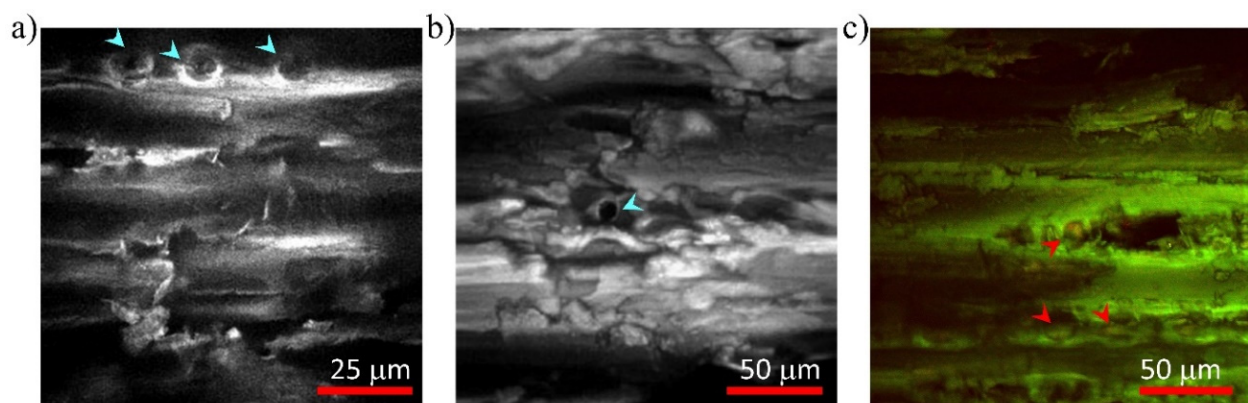
Figure 2. NLO microscopy images of poplar shavings cut along the direction of the stem on the tangential plane (excitation wavelength 840 nm). Bordered pits are pointed out by light-blue arrowheads. Greyscale intensity images (**a**) 100 × 100 μm^2 and (**b**) 200 × 200 μm^2 are obtained by optically summing all excited nonlinear signals, thus showing both SHG and TPEF signals indistinctively. (**c**) TPEF/SHG merged image (200 × 200 μm^2) enabling the distinction between TPEF (green-coded) and SHG (red-coded) signals, attributed to lignin and starch (pointed out by the red arrowheads), respectively.
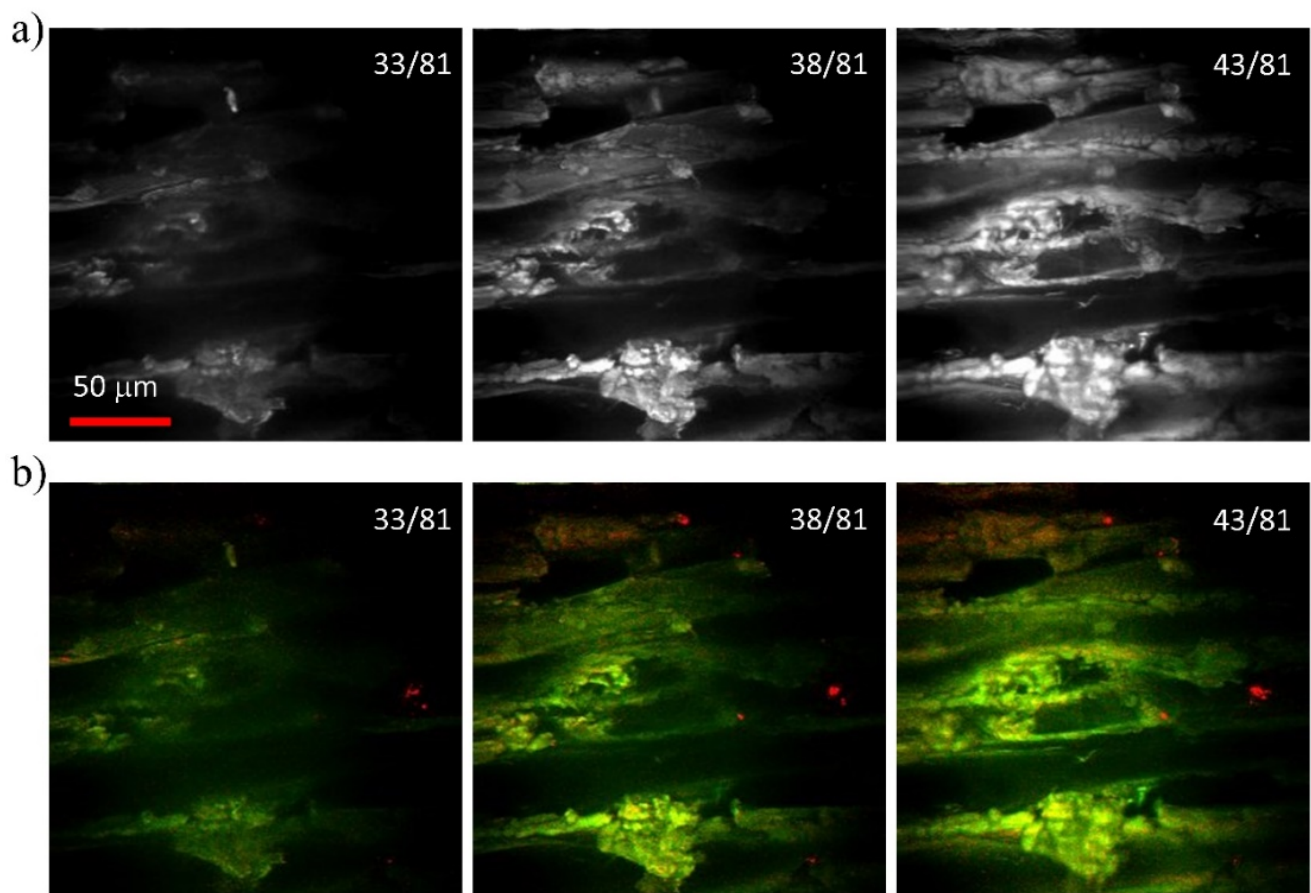
Figure 3. (**a**) Poplar greyscale NLO microscopy images ($200 \times 200 \ \mu m^2$) and (**b**) corresponding TPEF/SHG merged images acquired at different depths inside the wood slice (tangential section), highlighting the presence of SHG emitters. Depths of recording from the sample's surface are indicated in the top right corner (81 μm scanning depth; 1 μm sampling step).

A slightly more intense SHG signal was detected when imaging deeper into the sample, as shown in the combined TPEF/SHG stacks (Figure 3b), which are reported in comparison to the corresponding greyscale images (Figure 3a). In this case, the SHG signal is confined to small spots and is probably located in the secondary cell walls of vessels. Weaker signals are distributed in the upper part of the analyzed area.

3.2. Beech (Fagus sylvatica L.)

Vessels in beech can be found isolated or in the form of aggregates of 2–6 units. They are generally numerous and uniformly distributed inside the growth rings, with size ranging between 50 and 75 μm. Big and abundant pits between vessels are usually organized in horizontal lines. The parenchyma rays, which are generally composed of several series of cells (up to 25), are clearly visible in three of the analyzed areas, as shown in Figure 4a–c (FOV: $100 \times 100 \ \mu m^2$) (FOV: $200 \times 200 \ \mu m^2$). The TPEF/SHG axial stacks of the same area acquired with 5 μm steps are reported in Figure 4. Contrary to poplar, the SHG signal (red-coded) generated in beech is more widespread inside xylem and phloem cells, especially inside the rays and around the fibers, as demonstrated by larger red areas observed in the tangential sections reported here. Possible sources of the SHG signal are crystalline cellulose and particularly starch in the form of crystalline amylose, which is common in beech microstructures, specifically in the area underneath the bark (where this sample was extracted). The fluorescence signal from the cells is predominantly due to lignin, which is distributed in the secondary wall layers. In beech fibers, lignin

follows the direction of cellulose microfibrils closely, which are responsible for the lamellar structure [37].
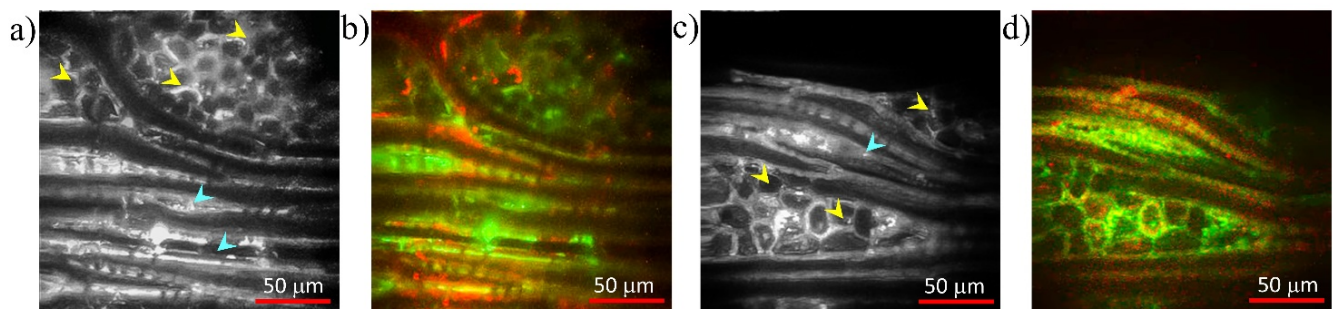
Figure 4. Beech NLO microscopy images (excitation wavelength 850 nm), showing the fibers (light-blue arrowheads) in the tangential section and the aggregates of parenchyma rays (yellow arrowheads) in the transverse section. Images are obtained from the maximum-intensity projection over all acquired images in a stack (101 μm scanning depth; 1 μm sampling step), thus enhancing the visualization of the inner details. (**a**,**c**) TPEF and SHG signals generated from lignin and cellulose/starch are optically summed. (**b**,**d**) Merged TPEF/SHG image showing the morphology of rays and fibers, as well as the distribution of SHG and fluorescence emitters.

3.3. Chestnut (Castanea sativa M.)

The microstructure in chestnut shavings is characterized by vessels (size of around 10 μm) arranged in oblique lines, which are typical of the latewood region. Conversely, earlywood is characterized by considerably larger vessels forming porous circles of 300–500 μm diameter. Pits between cells, which are larger in chestnut wood than in poplar and beech, were not observed in the analyzed samples. External deformations of parenchyma radial and axial cells, partially occluding adjacent vessels, were observed in the tangential shaving inside the transverse section of the parenchyma rays (Figure 5). These conformations were identified as tyloses, which are common in chestnut species. In the analyzed samples, an SHG signal, possibly emitted by crystalline cellulose, was detected mainly in small aggregates, as observed in Figure 5a,c.
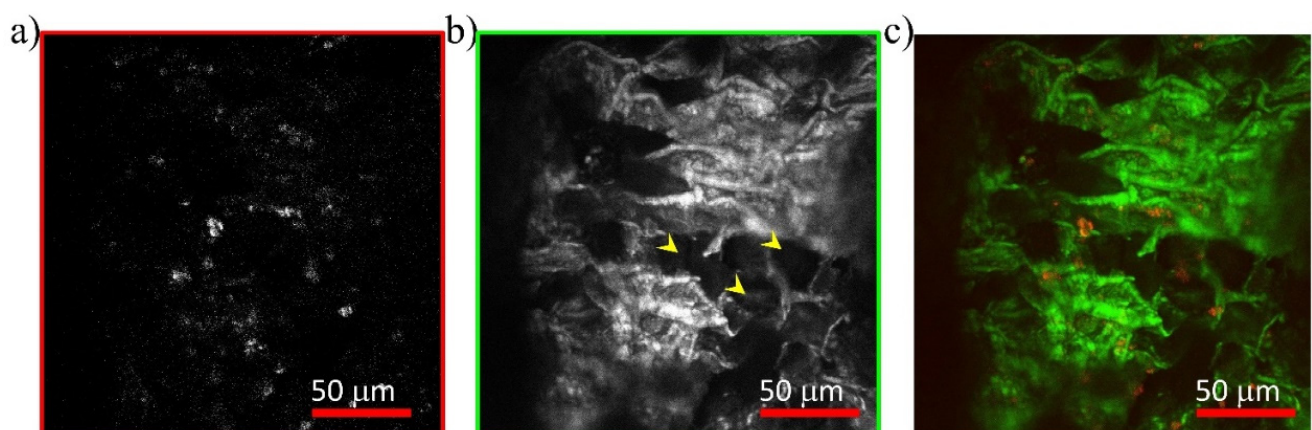
Figure 5. (**a**) SHG, (**b**) TPEF, and (**c**) merged TPEF/SHG images of chestnut acquired using an excitation wavelength of 800 nm, a FOV of 200 × 200 μm², and a resolution of 1024 × 1024 pixels. Tyloses (pointed out by the yellow arrowheads) are visible inside the parenchyma rays.

The SHG signal is also evident in the TPEF/SHG image stack with orthogonal views xz and yz (Figure 6b), acquired over a depth of 80 μm using an axial step of 1 μm.
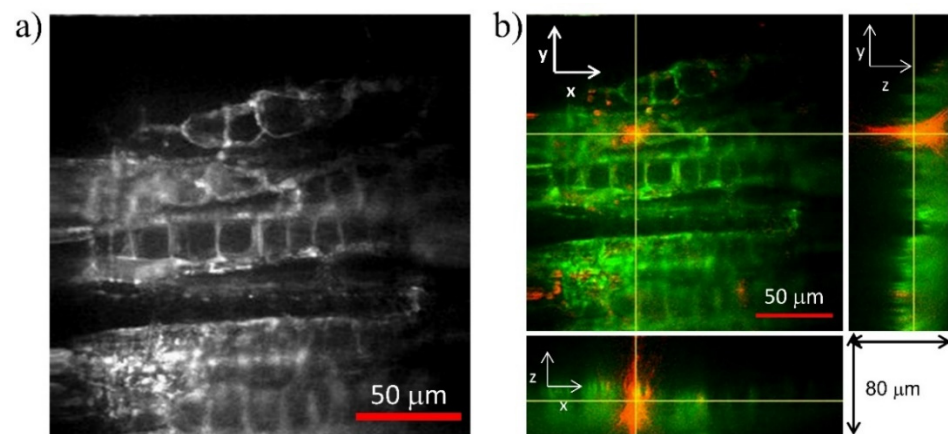
Figure 6. (**a**) Greyscale NLO microscopy image of chestnut and (**b**) orthogonal views of a merged TPEF/SHG image stack showing the presence of isolated aggregates of material strongly emitting SHG signals (red-coded) and TPEF signals (green-coded) generated by lignin.

4. Discussion

This study shows that the combined application of TPEF and SHG imaging offers a noninvasive and effective tool for clear visualization and differentiation of key microstructural features in different wood species. The 3D mapping allows for a qualitative discrimination/localization of the main molecular components of the cell walls (namely lignin, cellulose, and starch) due to their nonlinear optical properties. Such information is useful for comparing and characterizing different wood species, as well as for documenting the effects of aging and/or restoration treatments on wooden artwork at the microstructural level. The acquisition of nonlinear signals in the backward direction enables the analysis of samples of any thickness, thus enlarging the application of the method to a variety of objects. Moreover, it was demonstrated that well-resolved and well-contrasted TPEF/SHG images can be obtained from bulk wood samples with an air objective rather than a water-immersion one, despite a reduced NA. In this manner, liquid-sensitive and sometimes porous artwork materials can be fully preserved from damage. The use of polarization-resolved SHG imaging can be exploited to obtain quantitative information and to determine the orientation of cellulose microfibrils [38], thus improving their visibility in cell walls. Nonlinear microscopy can be profitably combined with coherent anti-Stokes Raman scattering (CARS) for a more comprehensive characterization of the chemical components, using the C=C vibration at 1600 cm^{-1} as a lignin marker and the C-O-C vibration at 1100 cm^{-1} as a cellulose marker [39]. It has already been shown that the integration of data obtained by TPEF-SHG and CARS enables the ability to monitor changes in cellulose supramolecular structure during enzymatic hydrolysis [40].

In addition, the level of unwanted fluorescence due to the crosstalk effect within the SHG channel should be considered in SHG/TPEF analyses. We evaluated the contribution of crosstalk on poplar samples from time-resolved measurements, resulting in approximately 5%. Although this is a small percentage of the overall signal, this effect can vary significantly across wood species and conditions and increase with excitation wavelength, as observed in [41]. Thus, a compromise between safety and crosstalk must be considered when choosing the excitation wavelength: shorter wavelengths, although potentially more dangerous, result in less fluorescence crosstalk in the SHG channel; longer wavelengths, although safer, cause higher crosstalk.

The reported results suggest that some of the effects of wood degradation can be monitored at the molecular level by combined TPEF/SHG imaging. Both weathering [42] and biological attack by fungi [43] cause an enrichment of the relative crystalline content of wood (cellulose) at the expense of the amorphous fractions (hemicellulose and lignin), with a concomitant increase in the size of crystallites and a reduction in molecular weight of cellulose due to thermo-oxidative processes [44]. Therefore, it is reasonable to expect that

this variation in the relative amounts of wood microcomponents could result in a change of ratios between TPEF and SHG signals and, specifically, an increase in the SHG signal from cellulose. The contributions of the individual components can be quantified by measuring the intensity of their respective NL signals (see Supplementary Materials). Monitoring the stability of signals over time would also allow for testing on the effectiveness of protective treatments on wooden artifacts. Since the effects of degradation can vary greatly by wood species, a comparative study of the most commonly used species for artwork production can be extremely useful.

5. Conclusions

This work paves the way for a systematic application of combined TPEF/SHG imaging on many wood species, which is necessary for a thorough characterization of the microstructures based on the nonlinear optical properties of the components. Considering that compact, flexible multiphoton microscopy systems have been already developed and successfully used in the biomedical field [45,46], a specific system allowing for in situ measurements of large objects is, without a doubt, feasible and highly suitable for the application of NLO analysis on works of art.

Supplementary Materials: The following supporting information can be downloaded at: https://www.mdpi.com/article/10.3390/photonics9030170/s1, Figure S1: NLO microscopy images of poplar (**a**–**c**), beech (**d**–**f**), chestnut (**g**–**i**) shavings cut in the tangential section along the stem length direction. Images were acquired under the same experimental conditions and with 840–850 nm excitation wavelength. The 8-bit grey-scale images are the individual channels (red = SHG, and green = TPEF) of the merged SHG/TPEF images (**c**,**f**,**i**), and show the contribution of SHG (**a**,**d**,**g**) and TPEF (**b**,**e**,**h**) signals as the intensity of light at each pixel in the dynamic range 0–255.

Author Contributions: Conceptualization, R.F., R.C. and A.D.F.; methodology, R.C., R.F. and A.D.F.; software, M.M.; validation, R.C. and R.F.; formal analysis, S.M., A.D.F. and E.B.; investigation, A.D.F. and S.M.; resources, R.C.; data curation, A.D.F., S.M. and E.B.; writing—original draft preparation, A.D.F.; writing—review and editing, A.D.F., R.C., A.G., R.F. and S.M.; visualization, M.M. and M.A.; supervision, R.F., R.C. and A.G.; project administration, R.F. and R.C.; funding acquisition, R.F. and R.C. All authors have read and agreed to the published version of the manuscript.

Conflicts of Interest: The authors declare no conflict of interest.

References

1. Stagno, V.; Egizi, F.; Corticelli, F.; Morandi, V.; Valle, F.; Costantini, G.; Longo, S.; Capuani, S. Microstructural features assessment of different waterlogged wood species by NMR diffusion validated with complementary techniques. *Magn. Reson. Imaging* **2021**, *83*, 139–151. [CrossRef]
2. Plötze, M.; Niemz, P. Porosity and pore size distribution of different wood types as determined by mercury intrusion porosimetry. *Eur. J. Wood Wood Prod.* **2011**, *69*, 649–657. [CrossRef]
3. Zhao, Y.; Man, Y.; Wen, J.; Guo, Y.; Lin, J. Advances in Imaging Plant Cell Walls. *Trends Plant Sci.* **2019**, *24*, 867–878. [CrossRef]
4. Jeffries, T.W. Physical, chemical and biochemical considerations in the biological degradation of wood. US Forest Products Laboratory. In *Wood and Cellulosics: Industrial Utilisation, Biotechnology, Structure and Properties*; Kennedy, J.F., Phillips, G.O., William, P.A., Eds.; Ellis Horwood Ltd.: Chichester, UK, 1988; Chapter 24; pp. 213–230.
5. Oltean, L.; Teischinger, A.; Hansmann, C. Influence of temperature on cracking and mechanical properties of wood during wood drying–A review. *BioResources* **2007**, *2*, 789–811.
6. Mizutani, G.; Sonoda, Y.; Sano, H.; Sakamoto, M.; Takahashi, T.; Ushioda, S. Detection of starch granules in a living plant by optical second harmonic microscopy. *J. Lumin.* **2000**, *87–89*, 824–826. [CrossRef]
7. Chu, S.-W.; Chen, I.-H.; Liu, T.-M.; Chen, P.C.; Sun, C.-K.; Lin, B.-L. Multimodal nonlinear spectral microscopy based on a femtosecond Cr:forsterite laser. *Opt. Lett.* **2001**, *26*, 1909–1911. [CrossRef]
8. Cox, G.; Moreno, N.; Feijó, J. Second-harmonic imaging of plant polysaccharides. *J. Biomed. Opt.* **2005**, *10*, 024013. [CrossRef]
9. Parodi, V.; Jacchetti, E.; Osellame, R.; Cerullo, G.; Polli, D.; Raimondi, M.T. Nonlinear Optical Microscopy: From Fundamentals to Applications in Live Bioimaging. *Front. Bioeng. Biotechnol.* **2020**, *8*, 585363. [CrossRef]

10. Gratton, E.; Barry, N.P.; Beretta, S.; Celli, A. Multiphoton fluorescence microscopy. *Methods* **2001**, *25*, 103–110. [CrossRef]
11. Denk, W.; Strickler, J.H.; Webb, W.W. Two-photon laser scanning fluorescence microscope. *Science* **1990**, *248*, 73–76. [CrossRef]
12. Hell, S.W.; Bahlmann, K.; Schrader, M.; Soini, A.; Malak, H.M.; Gryczynski, I.; Lakowicz, J.R. Three-photon excitation in fluorescence microscopy. *J. Biomed. Opt.* **1996**, *1*, 71–74. [CrossRef]
13. Gauderon, R.; Lukins, P.; Sheppard, C. Optimization of second-harmonic generation microscopy. *Micron* **2001**, *32*, 691–700. [CrossRef]
14. Oron, D.; Yelin, D.; Tal, E.; Raz, S.; Fachima, R.; Silberberg, Y. Depth-resolved structural imaging by third-harmonic generation microscopy. *J. Struct. Biol.* **2004**, *147*, 3–11. [CrossRef]
15. Fovo, A.D.; Castillejo, M.; Fontana, R. Nonlinear optical microscopy for artworks physics. *Riv. Nuovo Cim.* **2021**, *44*, 453–498. [CrossRef]
16. Mertz, J. Nonlinear microscopy: New techniques and applications. *Curr. Opin. Neurobiol.* **2004**, *14*, 610–616. [CrossRef]
17. Fovo, A.D.; Sanz, M.; Mattana, S.; Oujja, M.; Marchetti, M.; Pavone, F.; Cicchi, R.; Fontana, R.; Castillejo, M. Safe limits for the application of nonlinear optical microscopies to cultural heritage: A new method for in-situ assessment. *Microchem. J.* **2020**, *154*, 104568. [CrossRef]
18. Latour, G.; Echard, J.-P.; Soulier, B.; Emond, I.; Vaiedelich, S.; Elias, M. Structural and optical properties of wood and wood finishes studied using optical coherence tomography: Application to an 18th century Italian violin. *Appl. Opt.* **2009**, *48*, 6485–6491. [CrossRef]
19. Popescu, M.-C.; Popescu, C.-M.; Lisa, G.; Sakata, Y. Evaluation of morphological and chemical aspects of different wood species by spectroscopy and thermal methods. *J. Mol. Struct.* **2011**, *988*, 65–72. [CrossRef]
20. Brown, R.M., Jr.; Millard, A.C.; Campagnola, P.J. Macromolecular structure of cellulose studied by second-harmonic generation imaging microscopy. *Opt. Lett.* **2003**, *28*, 2207–2209. [CrossRef]
21. Psilodimitrakopoulos, S.; Amat-Roldan, I.; Loza-Alvarez, P.; Artigas, D. Estimating the helical pitch angle of amylopectin in starch using polarization second harmonic generation microscopy. *J. Opt.* **2010**, *12*, 084007. [CrossRef]
22. Psilodimitrakopoulos, S.; Gavgiotaki, E.; Melessanaki, K.; Tsafas, V.; Filippidis, G. Polarization Second Harmonic Generation Discriminates Between Fresh and Aged Starch-Based Adhesives Used in Cultural Heritage. *Microsc. Microanal.* **2016**, *22*, 1072–1083. [CrossRef]
23. Xue, Y.; Qiu, X.; Ouyang, X. Insights into the effect of aggregation on lignin fluorescence and its application for microstructure analysis. *Int. J. Biol. Macromol.* **2020**, *154*, 981–988. [CrossRef]
24. Djikanović, D.; Kalauzi, A.; Radotić, K.; Lapierre, C.; Jeremić, M. Deconvolution of lignin fluorescence spectra: A contribution to the comparative structural studies of lignins. *Russ. J. Phys. Chem. A* **2007**, *81*, 1425–1428. [CrossRef]
25. Donaldson, L. Softwood and Hardwood Lignin Fluorescence Spectra of Wood Cell Walls in Different Mounting Media. *IAWA J.* **2013**, *34*, 3–19. [CrossRef]
26. Donaldson, L. Autofluorescence in Plants. *Molecules* **2020**, *25*, 2393. [CrossRef]
27. Latour, G.; Echard, J.-P.; Didier, M.; Schanne-Klein, M.-C. In situ 3D characterization of historical coatings and wood using multimodal nonlinear optical microscopy. *Opt. Express* **2012**, *20*, 24623–24635. [CrossRef]
28. Donaldson, L.; Radotic, K. Fluorescence lifetime imaging of lignin autofluorescence in normal and compression wood. *J. Microsc.* **2013**, *251*, 178–187. [CrossRef]
29. Débarre, D.; Olivier, N.; Beaurepaire, E. Signal epidetection in third-harmonic generation microscopy of turbid media. *Opt. Express* **2007**, *15*, 8913. [CrossRef]
30. Dammström, S.; Salmén, L.; Gatenholm, P. On the interactions between cellulose and xylan, a biomimetic simulation of the hardwood cell wall. *BioResources* **2009**, *4*, 3–14.
31. Fujita, M.; Harada, H. Ultrastructure and formation of wood cell wall. In *Wood and Cellulosic Chemistry*; Hon, D.N.S., Shiraishi, N., Eds.; Marcel Dekker: New York, NY, USA, 2001.
32. Choat, B.; Cobb, A.R.; Jansen, S. Structure and function of bordered pits: New discoveries and impacts on whole-plant hydraulic function. *New Phytol.* **2008**, *177*, 608–626. [CrossRef]
33. Simmons, T.; Mortimer, J.; Bernardinelli, O.; Pöppler, A.-C.; Brown, S.; DeAzevedo, E.; Dupree, R.; Dupree, P. Folding of xylan onto cellulose fibrils in plant cell walls revealed by solid-state NMR. *Nat. Commun.* **2016**, *7*, 13902. [CrossRef]
34. Rencurosi, A.; Röhrling, J.; Pauli, J.; Potthast, A.; Jäger, C.; Pérez, S.; Kosma, P.; Imberty, A. Polymorphism in the Crystal Structure of the Cellulose Fragment Analogue Methyl 4-O-Methyl-β-D-Glucopyranosyl-(1-4)-β-D-Glucopyranoside. *Angew. Chem. Int. Ed.* **2002**, *41*, 4277–4281. [CrossRef]
35. Berti, S.; Fioravanti, M.; Macchioni, N. *La Struttura Anatomica del Legno ed il Riconoscimento dei Legnami Italiani di Più Ricorrente Impiego*; Berti, N., Ed.; CNE-INVALSA: Sesto Fiorentino, Italy, 2006.
36. Marchetti, M.; Baria, E.; Cicchi, R.; Pavone, F.S. Custom Multiphoton/Raman Microscopy Setup for Imaging and Characterization of Biological Samples. *Methods Protoc.* **2019**, *2*, 51. [CrossRef]
37. Fromm, J.; Rockel, B.; Lautner, S.; Windeisen, E.; Wanner, G. Lignin distribution in wood cell walls determined by TEM and backscattered SEM techniques. *J. Struct. Biol.* **2003**, *143*, 77–84. [CrossRef]
38. Nadiarnykh, O.; LaComb, R.B.; Campagnola, P.J.; Mohler, W.A. Coherent and incoherent SHG in fibrillar cellulose matrices. *Opt. Express* **2007**, *15*, 3348–3360. [CrossRef]

39.　Chen, B.-C.; Sung, J.; Lim, S.-H. Chemical Imaging with Frequency Modulation Coherent Anti-Stokes Raman Scattering Microscopy at the Vibrational Fingerprint Region. *J. Phys. Chem. B* **2010**, *114*, 16871–16880. [CrossRef]

40.　Peciulyte, A.; Kiskis, J.; Larsson, P.T.; Olsson, L.; Enejder, A. Visualization of structural changes in cellulosic substrates during enzymatic hydrolysis using multimodal nonlinear microscopy. *Cellulose* **2016**, *23*, 1521–1536. [CrossRef]

41.　Tai, H.-C.; Chen, P.-L.; Xu, J.-W.; Chen, S.-Y. Two-photon fluorescence and second harmonic generation hyperspectral imaging of old and modern spruce woods. *Opt. Express* **2020**, *28*, 38831–38841. [CrossRef]

42.　Lionetto, F.; Del Sole, R.; Cannoletta, D.; Vasapollo, G.; Maffezzoli, A. Monitoring Wood Degradation during Weathering by Cellulose Crystallinity. *Materials* **2012**, *5*, 1910–1922. [CrossRef]

43.　Howell, C.; Hastrup, A.C.S.; Goodell, B.; Jellison, J. Temporal changes in wood crystalline cellulose during degradation by brown rot fungi. *Int. Biodeterior. Biodegrad.* **2009**, *63*, 414–419. [CrossRef]

44.　Budrugeac, P.; Emandi, A. The use of thermal analysis methods for conservation state determination of historical and/or cultural objects manufactured from lime tree wood. *J. Therm. Anal.* **2010**, *101*, 881–886. [CrossRef]

45.　Cicchi, R.; Kapsokalyvas, D.; Stampouli, D.; De Giorgi, V.; Massi, D.; Lotti, T.; Pavone, F.S. In-vivo tissue imaging using a compact mobile nonlinear microscope. In Proceedings of the Multiphoton Microscopy in the Biomedical Sciences X, San Francisco, CA, USA, 23–28 January 2011; Volume 7569, p. 756930. [CrossRef]

46.　König, K. High-resolution multimodal clinical multiphoton tomography of skin. In Proceedings of the Photonic Therapeutics and Diagnostics VII, San Francisco, CA, USA, 22–27 January 2011; Volume 7883, p. 78830D. [CrossRef]